Scientific Contributions Oil & Gas, Vol. 48. No. 2, August: 363 - 377

SCIENTIFIC CONTRIBUTIONS OIL AND GAS
Testing Center for Oil and Gas
LEMIGAS

Journal Homepage:http://www.journal.lemigas.esdm.go.id
ISSN: 2089-3361, e-ISSN: 2541-0520

# Effects of Homogeneous and Heterogeneous Mineralogy in Carbonate Acidizing

Wahyu Sutresno

Department of Petroleum Engineering, Faculty of Technic, Bhayangkara Jakarta Raya University
Raya Perjuangan Street No. 81 Marga Mulya, North Bekasi

Corresponding author: wahyusutresno11@gmail.com.

Manuscript received: May 22th, 2025; Revised: June 16th, 2025
Approved: June 18th, 2025; Available online: June 26th, 2025; Published: June 27th, 2025.

**ABSTRACT** - A series of carbonate acidizing coreflood experiments using HCl was conducted on core samples from the Kujung Formation, offshore Northwest Java. Using XRD, SEM, and thin-section petrography, these samples were characterized as exhibiting varying degrees of heterogeneity. X-ray diffraction analysis showed that core plug Sample 7 consists of about 93% calcite, 3% dolomite, and 1–2% gypsum and pyrite, whereas core plug Sample 2 contains nearly 99% calcite. Mineralogical heterogeneity can affect the success of acidizing stimulation by determining the geometry (shape and size) of the wormholes that form. In addition to mineralogical heterogeneity, the presence of impurities in the rock may also influence the acidizing process and its outcomes. Conversely, in more homogeneous carbonate samples, a more uniform acid attack is observed. In homogeneous samples, carbonate dissolution was found to extensively "clean" clays and fine particles from the pore space. This study is expected to demonstrate different processes for enhancing permeability and porosity when using core samples of heterogeneous versus homogeneous mineralogy in carbonate acidizing applications.

**Keywords:** carbonate acidizing, coreflood experiment, mineralogy heterogeneity, wormhole geometry.



**How to cite this article:**

Wahyu Sutresno, 2025, Effects of Homogeneous and Heterogeneous Mineralogy in Carbonate Acidizing, Scientific Contributions Oil and Gas, 48 (2) pp. 363-377. DOI org/10.29017/scog.v48i2.1820.

## INTRODUCTION

Well stimulation techniques are crucial for maximizing hydrocarbon recovery and enhancing the productivity of oil and gas wells. Among these, matrix acidizing stands out as a widely adopted method (Turnip et al. 2024). This process involves injecting an acid into the reservoir formation, where it reacts with and dissolves specific minerals, thereby increasing the permeability of the rock. Matrix acidizing treatments are typically categorized based on the rock type being stimulated: carbonate or sandstone. Carbonate acidizing specifically targets the dissolution of calcite ($CaCO_3$) and dolomite ($MgCO_3$). Carbonate reservoir rocks are often classified by their calcite-to-dolomite ratio, with

those exceeding 50% calcite generally referred to as limestone. In contrast, sandstone acidizing primarily focuses on removing wellbore damage. While various fluids have proven effective as acidizing agents (Fredd & Fogler 1996), the successful design of a matrix treatment hinges on a careful consideration of both the damage mechanism and the rock type, as carbonate and sandstone reservoirs respond differently to acid treatments (Patton et al. 2003; Siregar & Wibowo 2019).

A key objective of acidizing is to improve permeability by creating conductive channels known as wormholes. The morphology of these wormholes is influenced by several factors, including the mineralogical heterogeneity of the rock, the specific acid used, the temperature, and the acid injection rate.

The heterogeneity of the reservoir plays a critical role in the success of acidizing treatments due to its direct impact on the damage removal mechanisms and, consequently, the dissolution pattern within the matrix (Wibowo 2013). Standard acid treatments, such as 15% HCl, are commonly employed to dissolve carbonate minerals and address plugging agents such as silicates, clays, gypsum, and feldspars. At a microscopic level, mineralogical heterogeneity can significantly influence the effectiveness of acidizing stimulation by dictating the shape and size of the formed wormholes. Beyond general heterogeneity, the presence of impurities within the rock constituents can also substantially affect the acidizing process and its outcomes, as different impurities react uniquely with the injected acid.

Furthermore, the texture pattern of the rock can also influence stimulation results, necessitating an analysis of the stimulation process from both microscopic and macroscopic perspectives. The rock's texture is intricately linked to its depositional history, diagenesis, composition, and structural characteristics (Li 2004; Li et al. 2004). This comprehensive understanding of mineralogical and textural influences is vital for optimizing carbonate acidizing treatments.

Mineralogy is conventionally defined by the relative abundance of crystalline compounds, typically determined through techniques such as X-ray Diffraction (XRD) and petrographic analysis.

## METHODOLOGY

### Core characterization

Conventional carbonate core plug samples from the Kujung Formation (offshore Northwest Java) were used for the experiments. Each core plug measures approximately 2.41 cm in length and 3.84 cm in diameter. Prior to acidizing, the samples were thoroughly characterized. Each core plug (Sample 2 and Sample 7) underwent X-ray CT scanning for internal structure visualization, and laboratory analyses including thin-section petrography, SEM-EDX, and XRD to determine mineralogy and pore structure. Thin sections were prepared from the end pieces of each core for petrographic examination (see Figure 1 and Figure 2 for polarized light photomicrographs of Sample 2).

Core plug 2, identified as a homogeneous sample, exhibits moderate to poor sorting, with grain sizes ranging from fine silt to very fine sand. Petrographic analysis further confirmed that this specific core plug sample is limestone.

Dunham (1992) scheme, this limestone can be classified as red algae, large forams, and packstone. The texture for core plug sample 2 was classified as limestone, which shows a grain size range from 0.12 mm to 5.69 mm with a grain size mean of 1.43 mm. The rock is grain-supported with low to moderate grain abrasion, with the grain composition of the sample predominantly skeletal grains (mostly large forams, with additional red algae, echinoderms, corals, bryozoans, indeterminate bioclasts, small benthonic forams, and planktonic forams) and intraclasts. Carbonate mud is present in low quantities as the matrix of this rock. The main diagenetic processes identified under petrographic examination include compaction, replacement, cementation, and dissolution. Compaction is evidenced by rigid grain breakage. Replacement of unstable grains has created secondary minerals, including calcite, microspar, micrite, and pyrite. The precipitation of calcite represents cementation. Minor dissolution of unstable grains has created secondary porosity. See Figure 3 and Figure 4 for the polarization of the core plug Sample 7 below.

Lastly, visual porosity is identified in very poor quality (1.50%), which is contributed to by secondary intragranular and dissolution pore types. Some micro-porosities are observed within carbonate mud

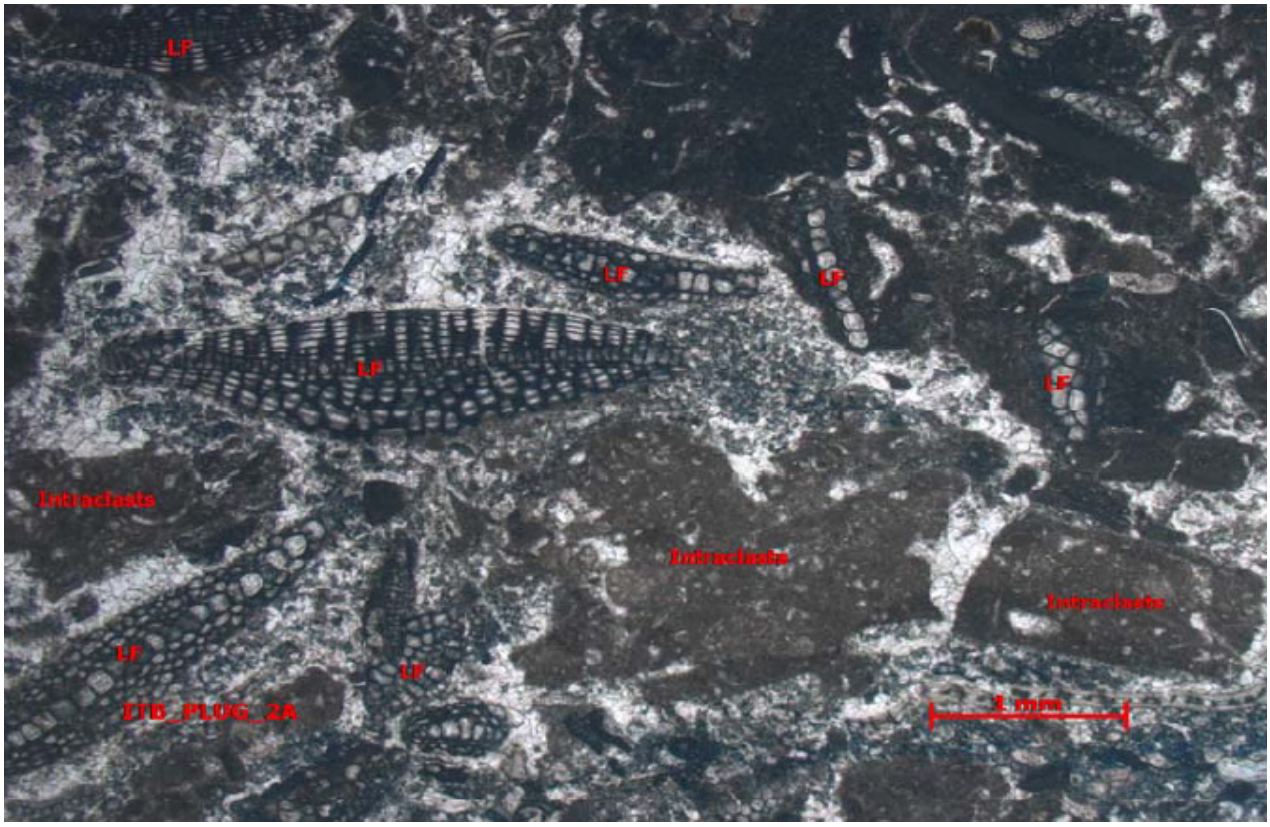


Figure 1. Core plug sample 2 polarization.

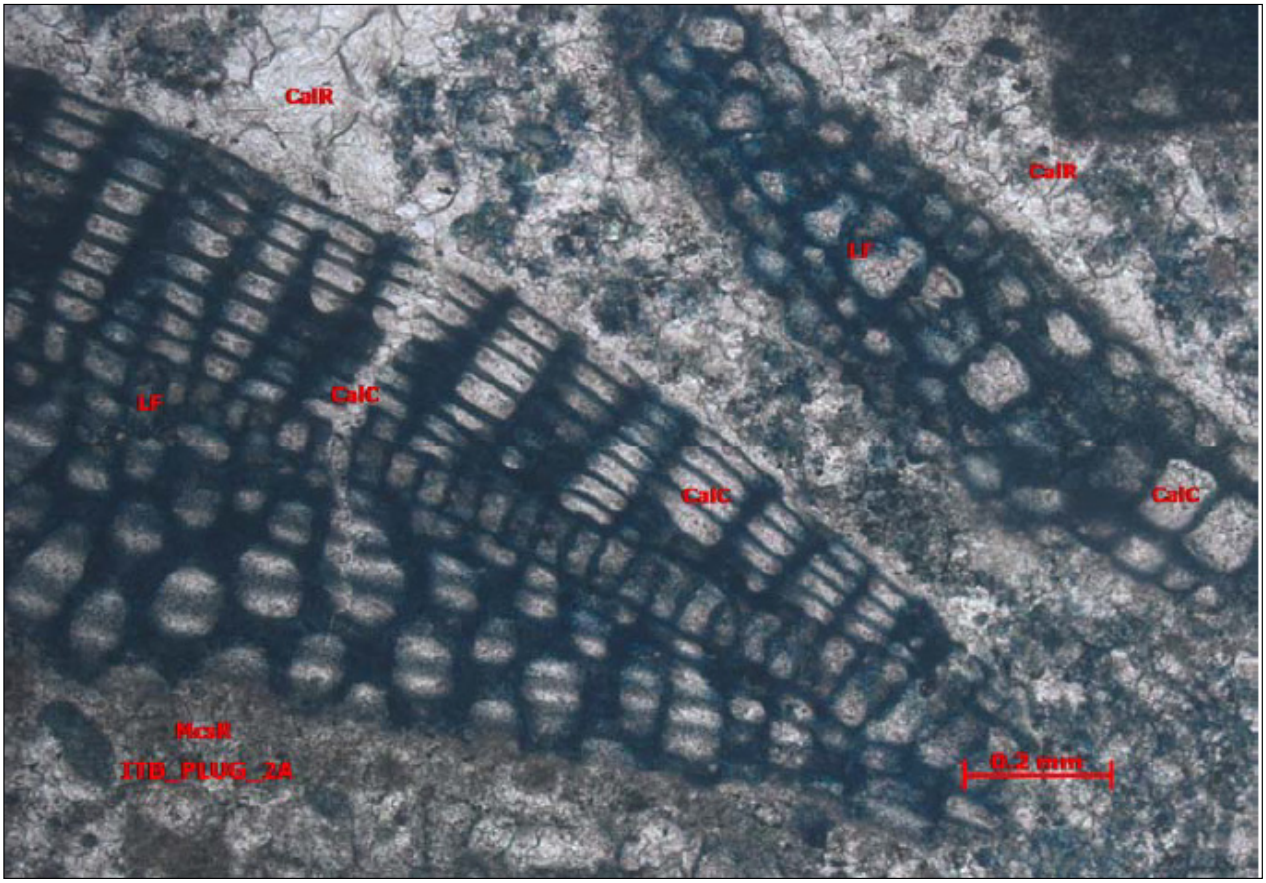


Figure 2. Core plug sample 2b polarization.

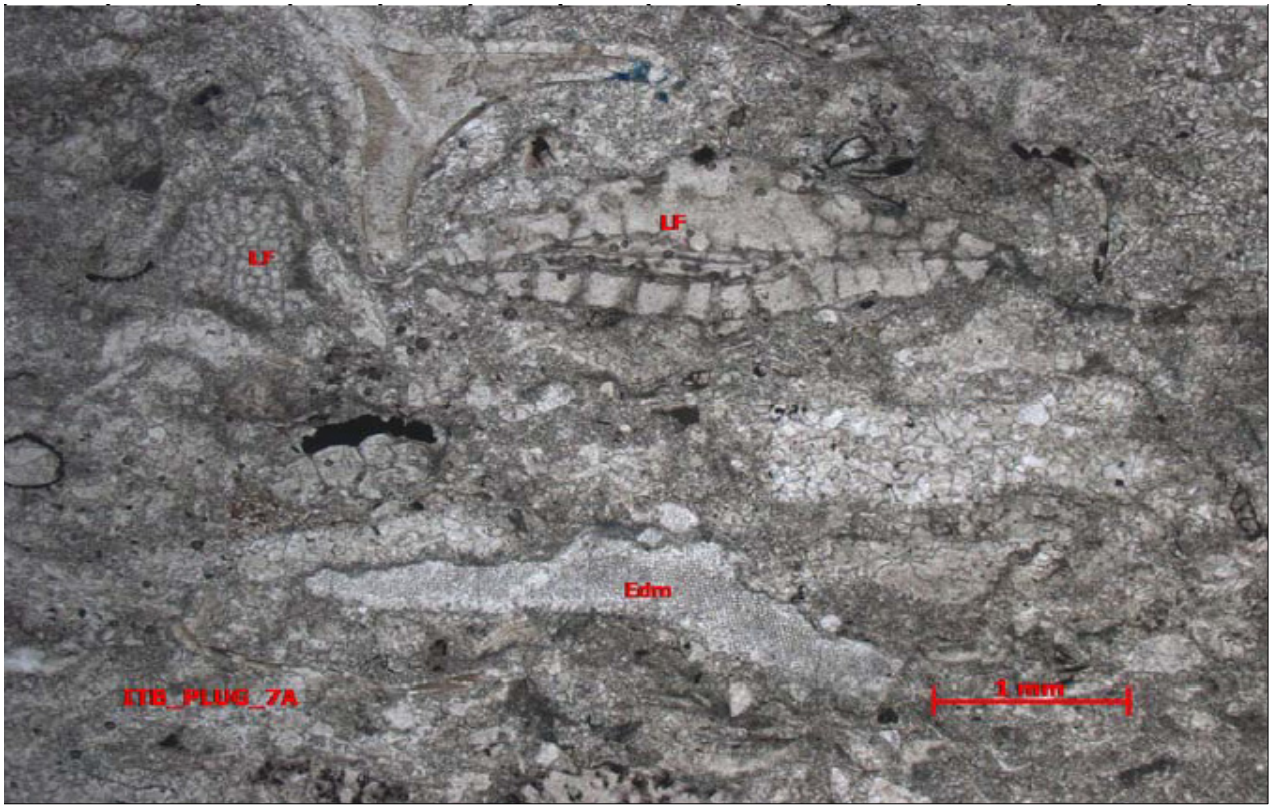


Figure 3. Coreplug sample 7a polarization.

and microspar. For the heterogeneity, the core plug Sample 7 is neomorphosed limestone. According to Dunham's (1962) modified scheme, this limestone can be classified as a neomorphosed wackestone. The texture of the coreplug sample is classified as limestone, which shows a grain size range from 0.05 mm to 3.20 mm with a grain size mean of 0.80 mm. The rock is matrix supported with moderate grain abrasion. Sedimentary structure is only represented by stylolite. The grain composition of the sample is predominantly skeletal grains (larger forams, corals, echinoderms, indeterminate bioclasts, molluscs, small benthonic forams, and bryozoan) with subordinate impurities of carbonaceous materials. Minor quantities of carbonate mud and locally clays are still detected as the original lime matrix, and an intensive neomorphism process in this rock is considered to have converted to calcite. The main diagenetic processes identified under petrographic examination include overburden compaction, replacement, cementation, and dissolution. Overburden compaction is reflected in recorded rigid grain breakage and stylolite. Replacement of unstable grains has created secondary minerals, including abundant calcite, along with lesser microspar, micrite, ferroan oxide, indeterminate clays, dolomite, pyrite, and siderite. Cementation is represented by precipitation of calcite, pyrite, and kaolinite. Minor dissolution of unstable grains has created secondary porosity. Lastly, visual porosity is identified in very poor quality (0.75%), which is contributed to by only the dissolution pore type.

**SEM–EDX analysis**

Scanning electron microscopy with energy-dispersive X-ray (SEM-EDX) analysis was performed to examine each sample's pore structure and mineral distribution at the microscopic scale. Prior to imaging, the sample chips were cleaned using organic solvents and ultrasonic agitation, then dried. Each sample piece was mounted on a 10 mm diameter copper stub and coated with a thin conductive layer of palladium alloy to prevent charging. The samples were then examined using a JEOL JSM-6390LA SEM instrument equipped with a digital imaging system and an EDX detector for elemental analysis.

The SEM observations corroborated the petrographic findings for both samples. Images of Sample 2 (see Figure 5) show a grain-supported limestone composed of diverse skeletal grains

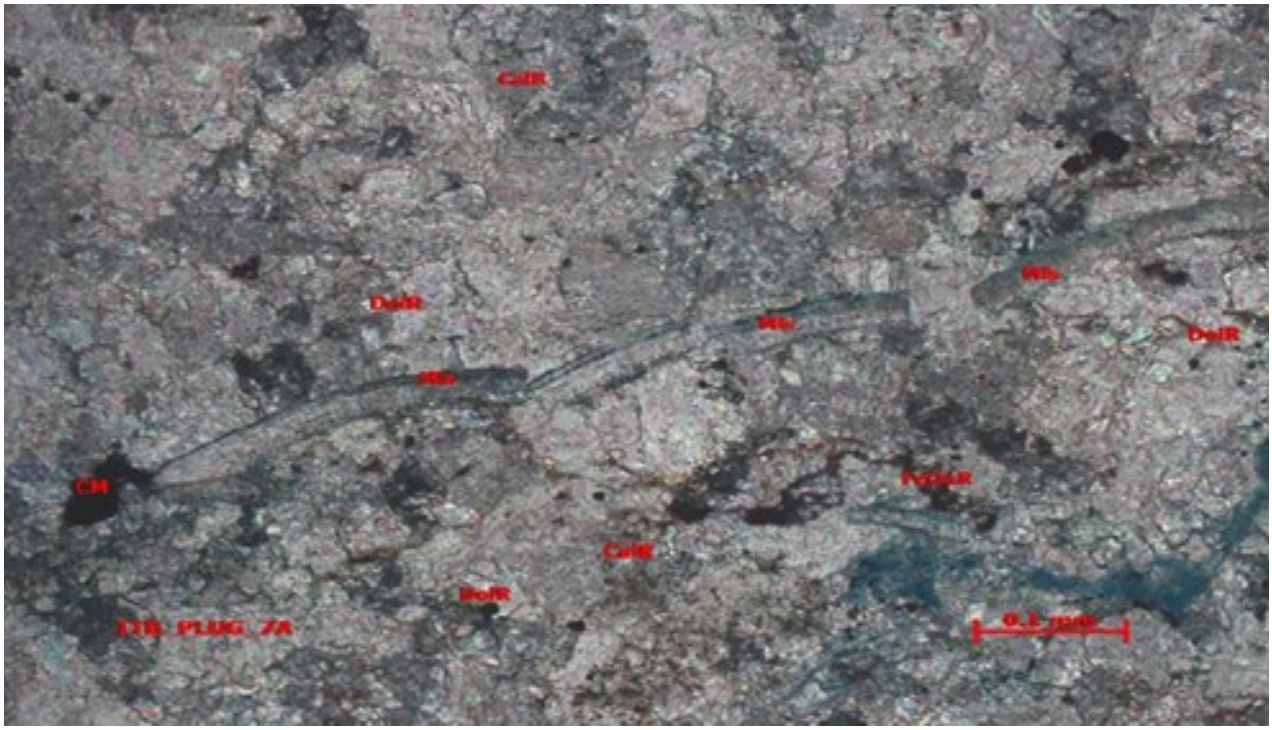


Figure 4. Core plug sample 7b polarization.

(planktonic and small benthonic forams, fragments of larger forams, and other bioclasts) set in a carbonate mud matrix. Diagenetic minerals such as calcite, micrite, and pyrite are observed replacing some of the original grains or filling pore spaces, consistent with the thin-section analysis. Overall, Sample 2 exhibits poor visual porosity, mainly in the form of micro- to meso-scale dissolution pores and micro-intercrystalline pores between calcite crystals. Higher-magnification SEM images (Figure 6) reveal that many of these dissolution pores have been almost filled by calcite cement, which reduces the effective porosity of the rock.

Similarly, SEM images of Sample 7 (Figure 8) indicate a matrix-supported limestone with skeletal grains (dominated by large foraminifera, along with fewer planktonic forams and other bioclasts) embedded in a calcitized mud matrix. The effects of diagenesis are evident, including extensive neomorphism of the original lime mud to calcite and minor precipitation of dolomite, pyrite, and kaolinite in the pore spaces. As in Sample 2, dissolution features in Sample 7 have generated some secondary pores; however, the overall visual porosity is very poor. Only micro- to meso-scale pores formed by dissolution are evident, often appearing as micro-intercrystalline voids among the fine calcite crystals (micrite and microspar). High-magnification views (see Figure 9 and Figure 10) show pervasive calcite recrystallization in the matrix and occasional microporosity between the newly formed calcite crystals, reflecting the intensive neomorphism and limited dissolution. Visual porosity is poor in quality, comprises mainly micro to meso dissolution porosities and micro-intercrystalline porosities developed between calcite. See Figure 5 below for Upper SEM Photomicrograph Core Plug Sample 2 with magnification to 150.

Lower SEM Photomicrograph core plug sample 2. Detailed SEM view shows dissolution porosity, which has been almost filled by calcite (see Figure 6). The occurrence of such cements causes a decrease in the porosity of the limestone. Magnification is up to 900.

Upper SEM Photomicrograph core plug sample 7. General SEM shows a matrix-supported limestone that is composed of skeletal grain components, including mostly large forams, lesser planktonic forams, and indeterminate bioclasts. The limestone has been affected by diagenetic events that consist of replacement from labile skeletal grains and carbonate mud matrix to calcite, micrite, and slightly dolomite and pyrite, followed by precipitation of minor kaolinite and pyrite; and dissolution of unstable

grains, which have yielded secondary porosity. Visual porosity is very poor in quality. It consists of micro to meso dissolution porosities and micro intercrystalline porosities distributed among crystals of calcite (mainly of the micrite and microspar). See Figure 8 below for Upper SEM Photomicrograph Core Plug Sample 7 with magnification to 150.

Lower SEM Photomicrograph Core Plug Sample 7. Detailed SEM view shows calcite (See Figure 9) as a product of the neomorphism process in the lime mud matrix. The adjoining grain (See Figure 10) has probably been micritized with the development of locally micro-pores between tiny calcite crystals. Magnification is up to 850.

**XRD (X-Ray diffraction)**

These measurements are expected to determine the amount of mineral content present in each core plug sample. It is particularly applicable to fine-grained sediments where a polarizing microscope would have difficulty in distinguishing individual mineral phases.

Firstly, the picked samples were washed using toluene to remove oil content and other contaminants. The washed samples were then dried and ground thoroughly into a <0.062 mm-sized powder. Afterward, the powder was placed and flattened into the sample holder, and was ready for bulk sample analysis. For clay treatment, the selected samples were weighed and disintegrated, then shaken firmly in Aquadest to obtain a homogeneous suspension. The solution was sonicated for about three minutes to disperse coarser grains from the solution. The silt and clay fraction was separated from the solution through a gravity settling procedure of approximately four hours, and the suspension was removed from the interval of five centimeters above. The solution was centrifuged to separate the silt and clay fraction from the liquid. The silt and clay fraction was then deposited onto a sample amount and air-dried. Clay treatment procedure consisted of three steps: 1) air-dried treatment, 2) treatment with ethylene glycol glycolated for smectite identification, and 3) heating to 550°C to distinguish kaolinite and chlorite. The presence of the particular minerals was determined qualitatively by comparing the recorded diffractogram proportion with standard references of minerals in the pre-installed powder data file of the International Center for Diffraction Database (ICDD). The proportion of each mineral was estimated semi-quantitatively (in weight percent) based on its peak intensity with reference procedures outlined by several workers (Weaver 1956; Jonas & Brown 1959; Reynolds 1980) and an empirical matrix correction applied for normalization. The XRD examination results are documented in Table 1 below.

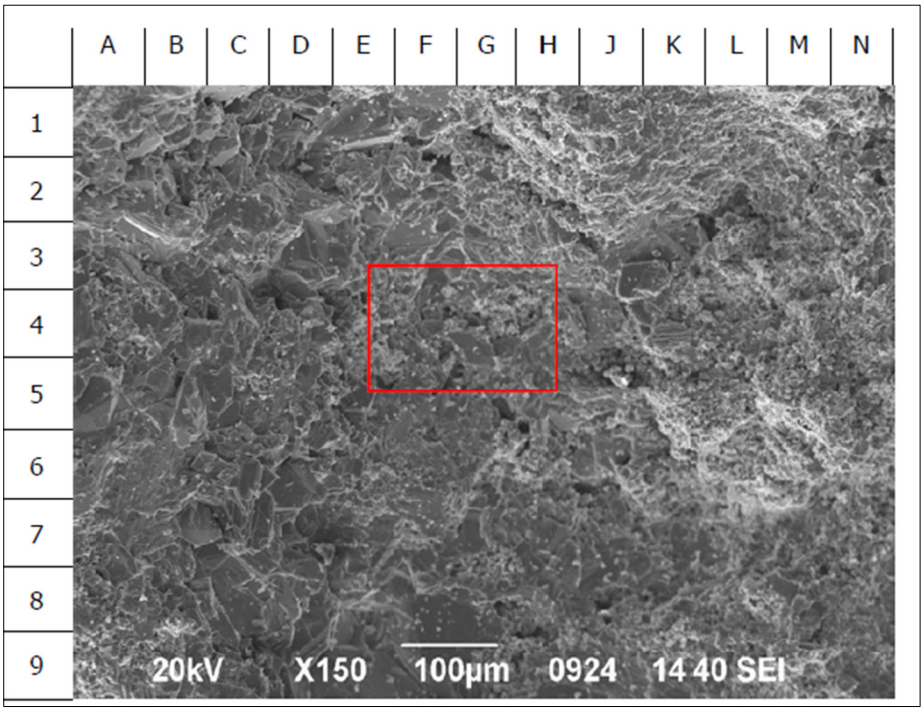


Figure 5. Upper SEM photomicrograph core plug sample 2 magnification up to 150.

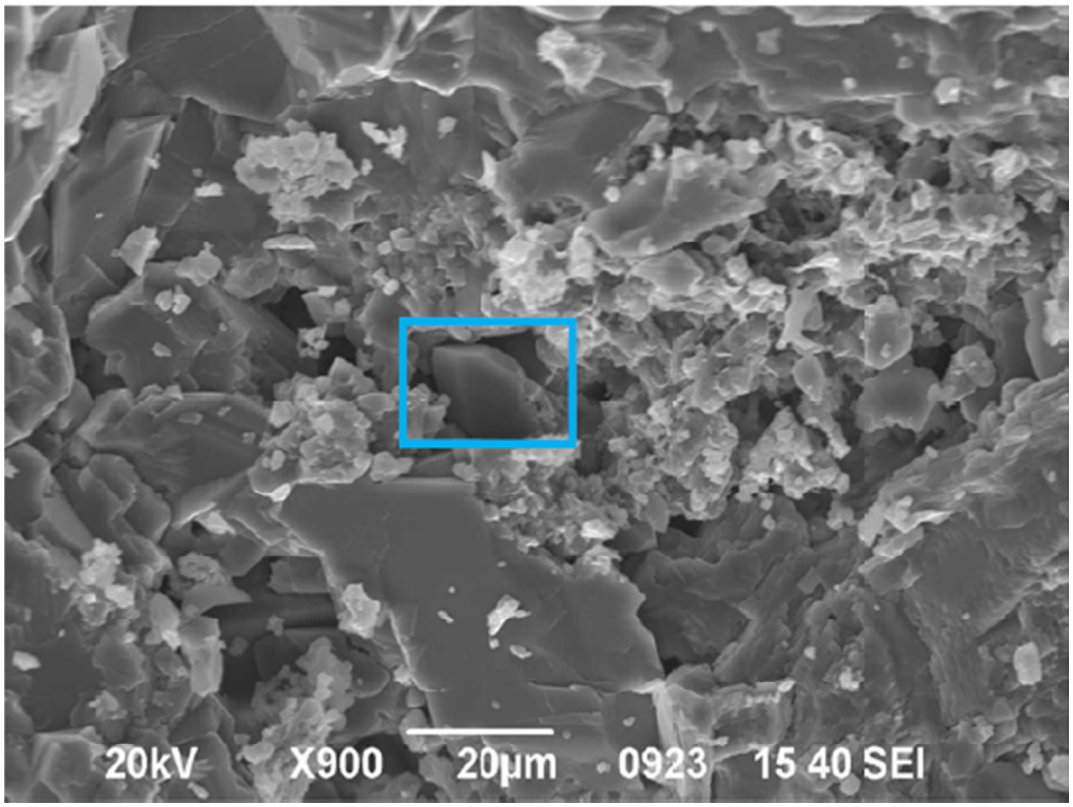


Figure 6. Lower SEM photomicrograph core plug sample 2 (calcite with cement) magnification up to 900.

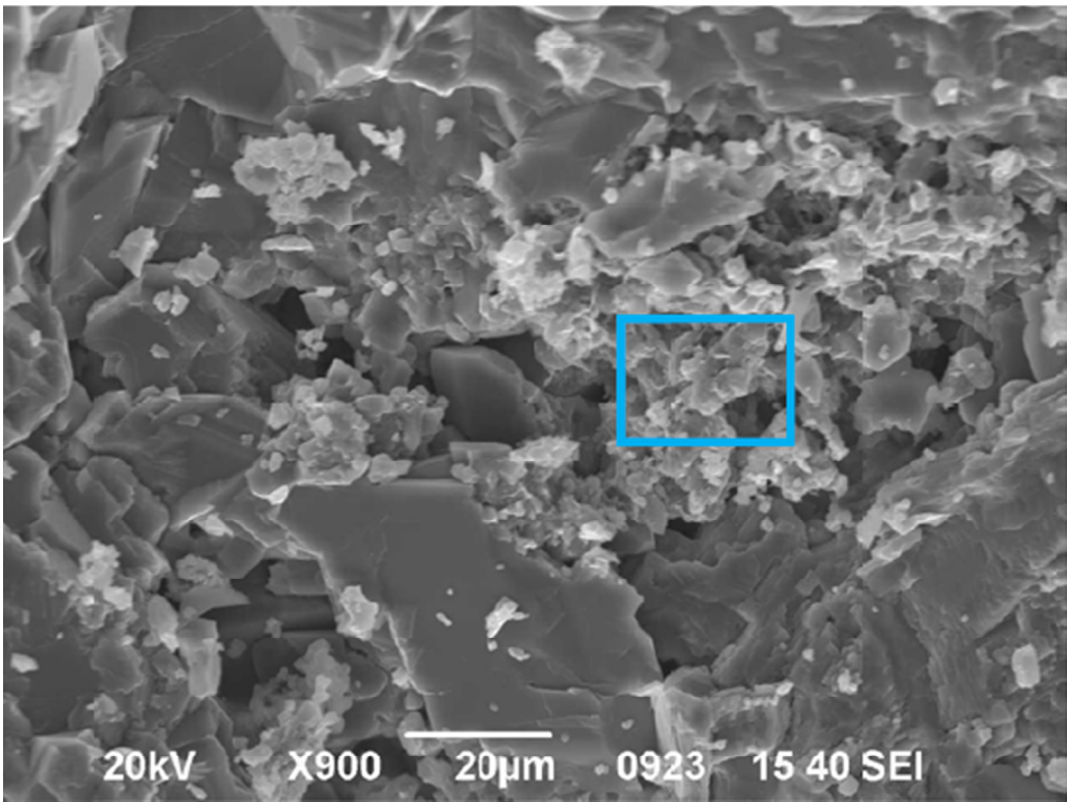


Figure 7. Lower SEM photomicrograph core plug sample 2 (calcite with siliceous quartz cement) magnification up to 900.

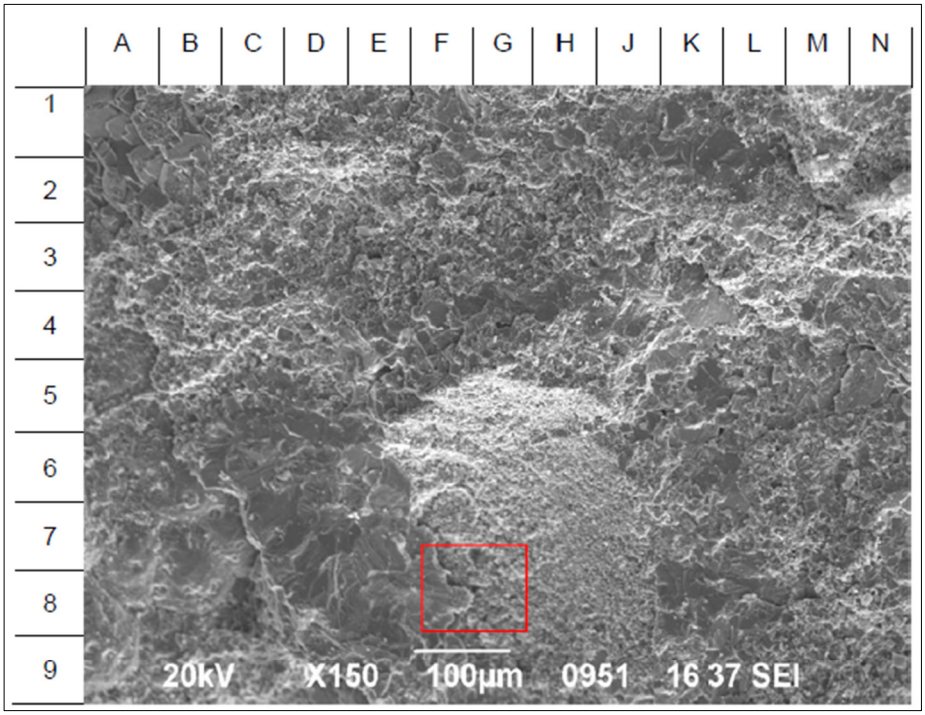


Figure 8. Upper SEM photomicrograph core plug sample 7 with magnification to 150.

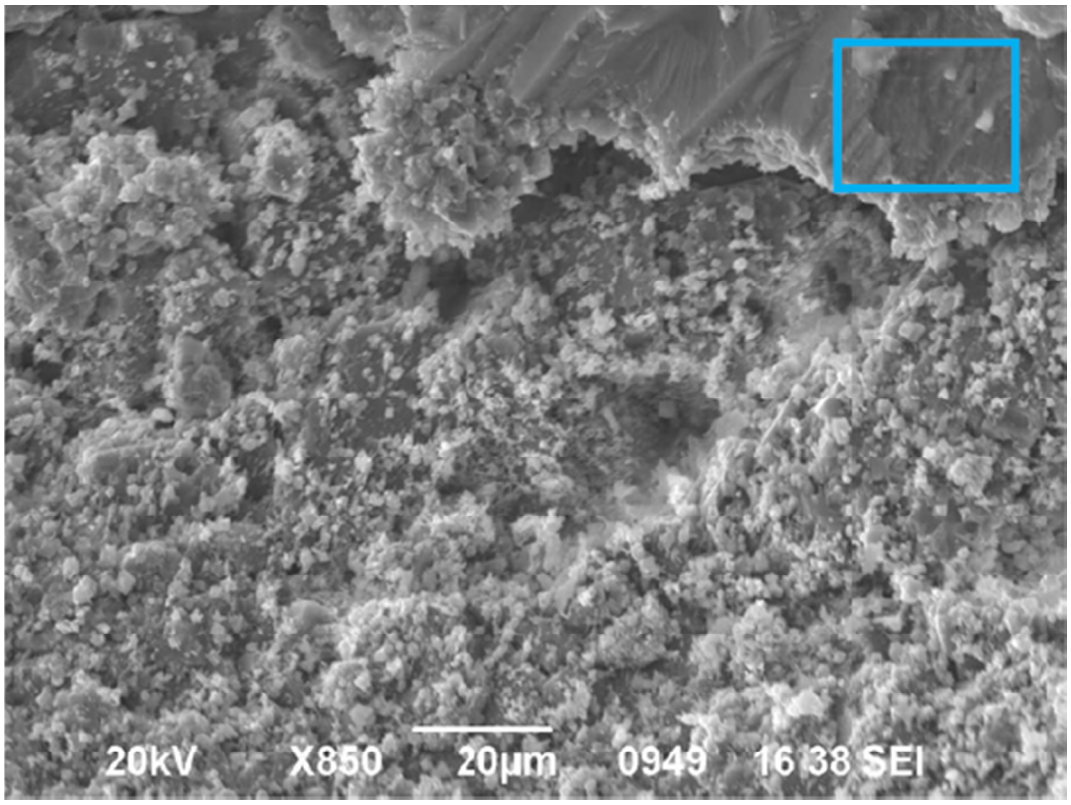


Figure 9. Lower SEM photomicrograph core plug sample 7 (neomorphosed calcite) magnification up to 850.

Table 1. XRD analyses for coreplug samples 2 and 7.

| | | Clay Minerals (%) | | | | | Crbonate Minerals (%) | | | Other Minerals (%) | | | | | | Total (%) | | | |
|---|---|---|---|---|---|---|---|---|---|---|---|---|---|---|---|---|---|---|---|
| No | Sample Code | Smectite | Illite_Smectite | Illite | Kaolinite | Chlorite | Calcite | Dolomite | Siderite | Quartz | Ankerite | Potash Fladspar | Plagiodase | Gypsum | Pyrite | Clay | Carbonate | Other | Remarks |
| 1 | 1 | - | - | - | - | - | 59.60 | - | | 20.2 | 20.2 | - | - | - | - | 0.00 | 59.60 | 40.40 | Coreplug |
| 2 | 2 | - | - | - | - | - | 99.00 | tr | - | 1.00 | - | - | - | - | - | 0.00 | 99.00 | 1.00 | Coreplug |
| 3 | 3 | 1.00 | - | - | - | - | 96.00 | - | - | 1.00 | - | - | - | 1.00 | 1.00 | 1.00 | 96.00 | 3.00 | Coreplug |
| 4 | 4 | tr | - | - | - | - | 97.00 | tr | - | 1.00 | - | - | - | - | 2.00 | 0.00 | 97.00 | 3.00 | Coreplug |
| 5 | 5 | - | - | - | - | - | 93.50 | - | - | 6.5 | - | - | - | - | - | 0.00 | 93.50 | 6.50 | Coreplug |
| 6 | 6 | - | - | - | - | - | 90.60 | - | - | 9.4 | - | - | - | - | - | 0.00 | 90.60 | 9.40 | Coreplug |
| 7 | 7 | - | tr | - | - | - | 93.00 | 3.00 | - | 1.00 | - | - | - | - | - | 0.00 | 96.00 | 4.00 | Coreplug |

Note: tr =trace

## Core flood

Before the acidizing experiments, the core plugs underwent a meticulous cleaning and preparation process. Initially, the core plugs were cleaned and extracted using toluene in a Soxhlet apparatus for a duration of 48 hours. Following this, the cores were thoroughly dried in an oven at 70ºC for an equivalent period.

The experimental setup utilized for the acid injection is schematically represented in Figure 10. For the injection phase, liquids were pumped through the prepared core samples using a positive displacement pump. This pump allowed for the delivery of fluids at various constant flow rates. A typical experimental procedure involved the following steps. Firstly, 15% HCL Fluid was applied into the piston tube up to 500 ml. After that, the operating temperature was set for the core holder to 70ºC (158ºF) on the temperature controller, and the confining pressure was set for the core holder to 230 psi (the confining pressure cannot exceed 230 psi, as this would cause a leak in the rubber seal inside the core holder). Next, after the core plug and fluid were ready at a temperature of 70ºC (158ºF), 15% HCl injection was carried out by setting the injection rate at the rust pump to 0.1 cc/min. Furthermore, the pressure change was recorded on the digital pressure gauge that was installed before the core holder every 1 minute from the start of the injection. In addition, the amount of fluid that came out of the tube every 1 minute was recorded. The difference between injection pressure and confining pressure was 10 psi. If the recorded injection pressure was close to 230 psi, the injection was stopped.

Matrix acidizing in carbonate rock was performed to observe the impact of HCl on two key relationships: pressure (P) versus injection time of the acid. The main purpose is to observe the wormhole changes produced by the dissolution of minerals through permeable channels due to the effect of the HCl for both samples (see Figure 12 and Figure 13).

Figures 12 and 13 illustrate the pressure drop observed across the core during the injection of a 15% HCl solution at a constant rate of 0.010 cc/min. Once a breakthrough occurred, the core flood apparatus recorded a low and constant pressure drop, indicating that the fluid was effectively flowing through the newly created wormhole structures.

Throughout the core flood testing, the pressure drop across the rock was continuously measured as the dissolution process advanced. From these measurements, the average permeability of the rock was calculated using Darcy's Law. The comprehensive results of these experiments are summarized in Table 2.

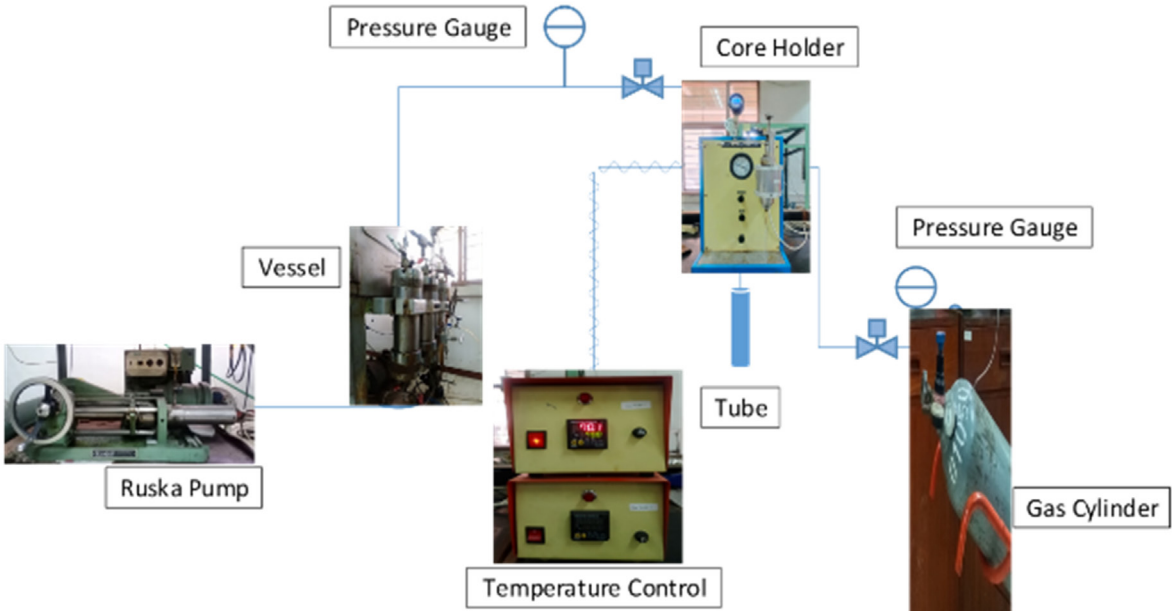


Figure 11. Coreflood diagram

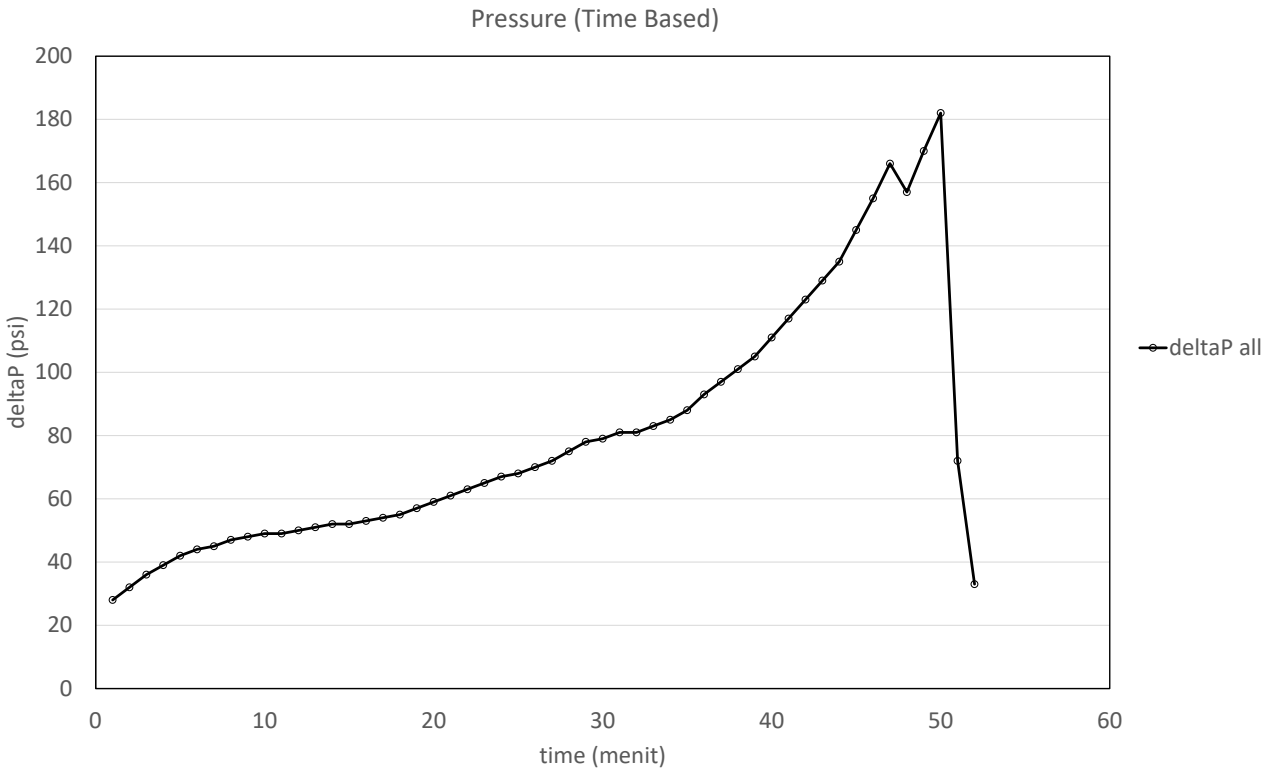


Figure 12. Time Vs pressure coreplug sample 2.

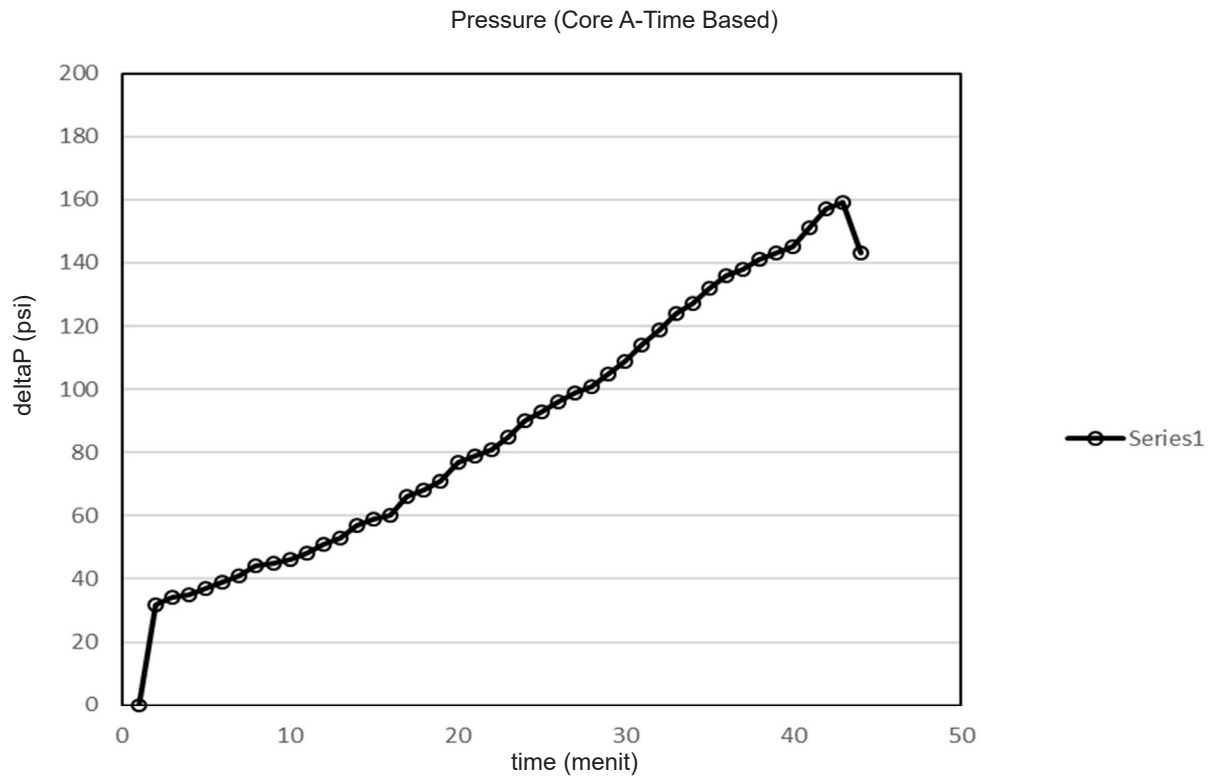


Figure 13. Time Vs pressure coreplug sample 7.

Table 2. Summary of porosity and permeability coreplug sample 2 and 7 before and after injection.

| BEFORE INJECTION | | | | | | | | | | | | | |
|---|---|---|---|---|---|---|---|---|---|---|---|---|---|
| BASIC INFORMATION | | | | | | Confining Pressure = 0 (psi) | | | Confining Pressure = 230 psi | | | | |
| Sample code | D | L | W | GD | Vg | BV | PV | φ | BV | PV | φ | Ka | KKlinken |
| | mm | mm | gr | gr/cc | cc | cc | cc | % | cc | cc | % | mD | mD |
| 2 | 25.550 | 37.850 | 46.350 | 2.702 | 17.151 | 19.406 | 2.255 | 11.620 | 18.352 | 1.57 | 6.545 | 0.18328 | 0.03199 |
| 7 | 25.320 | 39.820 | 52.469 | 2.733 | 19.200 | 20.050 | 0.850 | 4.240 | 19.460 | 0.260 | 1.338 | 0.070 | 0.008 |
| AFTER INJECTION | | | | | | | | | | | | | |
| 2 | 25.55 | 37.85 | 45.41 | 2.69 | 16.86 | 19.41 | 2.55 | 13.13 | 18.43 | 1.57 | 8.53 | 0.693 | 0.339 |
| 7 | 25.32 | 39.82 | 52.37 | 2.72 | 19.25 | 20.05 | 0.80 | 3.97 | 19.68 | 0.43 | 2.16 | 0.06014 | 0.00635 |

## RESULT AND DISCUSSION

Performance of homogeneous vs. heterogeneous samples is compared. As shown by the experimental results (Table 2), acidizing had markedly different effects on the two core samples. Sample 2 (homogeneous mineralogy) exhibited a significantly greater increase in permeability and a more pronounced porosity enhancement after acid injection compared to Sample 7 (heterogeneous mineralogy). This contrast underscores the important role of rock composition in acidizing effectiveness. In particular, the proportion of carbonate minerals versus impurities directly influences acid penetration depth and wormhole propagation (Allen & Roberts, 1993). In Sample 2, the abundance of calcite facilitated rapid acid breakthrough and efficient wormhole formation. Consequently, the ratio of final to initial permeability in Sample 2 was much higher than in Sample 7. The nearly pure calcite in Sample 2 readily dissolved in HCl, producing extensive wormholes and large permeability gains, whereas the presence of acid-insoluble minerals in Sample 7 limited the extent of dissolution and permeability improvement. The before-and-after data indicate that a homogeneous carbonate rock can achieve far greater increases in porosity and permeability during acidizing than a heterogeneous carbonate (Santosa & Putra, 2018).

In more heterogeneous carbonate formations such as Sample 7, the acid tends to preferentially travel through existing higher-permeability pathways, leaving the low-permeability regions largely unstimulated. As a result, Sample 7 experienced a slower acid breakthrough and only a minor improvement in overall permeability. This outcome is primarily attributed to the presence of impurities (e.g., clays and other siliceous minerals) blocking pore throats and hindering wormhole development. Carbonate reservoir rocks are often not pure limestone. Those commonly contain significant fractions of siliceous materials (quartz, mica, feldspar, and clay minerals such as kaolinite, illite, smectite, and chlorite) that do not react with hydrochloric acid. Since the acids used in carbonate stimulation are essentially ineffective at dissolving these siliceous constituents, the impurities remain in place and continue to impede fluid flow. In Sample 7, such undissolved materials likely contributed to the much smaller permeability increase observed after acidizing.

## CONCLUSION

This study investigated the effects of mineralogical homogeneity versus heterogeneity on carbonate matrix acidizing using core samples from the Kujung Formation. The results demonstrate that the mineralogical makeup of a carbonate rock has a profound impact on the success of acidizing treatments.

The homogeneous carbonate sample (Sample 2), composed predominantly of calcite, exhibited a much faster acid breakthrough and a greater increase in both permeability and porosity after acid treatment. This high stimulation efficiency is attributed to hydrochloric acid's ability to readily react with and dissolve the abundant calcite, leading to the rapid development of an interconnected wormhole network. These conductive channels significantly enhance fluid flow through the rock, thereby improving reservoir productivity.

In contrast, the heterogeneous carbonate sample (Sample 7) showed a substantially delayed acid breakthrough and, critically, little to no improvement in permeability following acid injection. The presence of impurities and siliceous minerals—identified in this sample through petrographic and SEM-EDX analyses greatly diminished the acid's effectiveness. Since HCl could not dissolve these siliceous components (such as clays, quartz, and other non-carbonate constituents), they remained intact within the pore structure, preventing significant wormhole formation and permeability enhancement. Thus, mineralogical heterogeneity, especially the inclusion of acid-insoluble constituents, can severely limit the efficacy of carbonate acidizing treatments.

## ACKNOWLEDGEMENT

We would also like to thank PT. Pertamina Hulu Energi WMO for supporting the experimental work.

## GLOSSARY OF TERMS

| Symbol | Definitions | Unit |
|---|---|---|
| HCl | *Hydrochloric acid is used as a stimulation fluid* | – |
| Acidizing | *Well stimulation technique, injecting acid to improve* | – |

| | | |
|---|---|---|
| | *permeability* | |
| Matrix Acidizing | *Low-pressure acid injection technique to dissolve formation damage* | – |
| Carbonate Rock | *Reservoir rock is mainly composed of calcite and dolomite* | – |
| Calcite ($CaCO_3$) | *Primary carbonate mineral in reservoir rock* | – |
| Dolomite ($CaMg(CO_3)_2$) | *Carbonate minerals are often present in carbonate reservoirs* | – |
| pH | *Measure of acidity of the solution* | *[–]* |
| μ | *Viscosity of acid solution* | *cP* |
| T | *Temperature in coreflood experiments* | *°C* |
| C | *Acid concentration* | *M (mol/L)* |
| PVbt | *Pore volume to breakthrough; volume of acid required for breakthrough* | *PV (pore volumes)* |
| ϕ (phi) | *Porosity of the rock sample* | *[%]* |
| k | *Absolute permeability of the rock* | *mD* |

## REFERENCES


Allen, T.O. & Roberts, A.P., 1993, Production operations. 5th ed. Tulsa, OK: OGCI Publications.

Barri, A.A., Al-Musabah, A.S., Al-Muntasheri, G.A., & Al-Ameri, S.S., 2015. Effect of stimulation with chelating agents on carbonate rocks integrity. In: SPE Middle East Oil & Gas Show and Conference. Manama, Bahrain: SPE. doi:10.2118/172709-MS.

Bazin, B., & Ben-Naceur, K., 1995, A laboratory evaluation of acid propagation in relation to acid fracturing: Results and interpretation. In: European Formation Damage Conference. The Hague, Netherlands: SPE. doi:10.2118/30085-MS.

Bazin, B., Roque, C., & Bouteca, M., 1996. Improvement in the characterization of acid wormholing by in situ X-ray CT visualizations. In: SPE International Symposium on Formation Damage Control. Lafayette, Louisiana: SPE. doi:10.2118/31073-MS.

Burton, R.C., Nozaki, M., Zwarich, N.R., & Furui, K., 2018, Improved understanding of acid wormholing in carbonate reservoirs through laboratory experiments and field measurements. In: SPE Annual Technical Conference and Exhibition. Dallas, Texas, USA: SPE. doi:10.2118/191625-MS.

Cohen, C.E., Barthel, F. & Ben-Naceur, K., 2007, A new matrix-acidizing simulator based on a large-scale dual-porosity approach. In: European Formation Damage Conference. Scheveningen, Netherlands: SPE. doi:10.2118/107755-MS.

De Oliveira, T.J.L., Schechter, D.S., & Pires, A.P., 2012, Numerical simulation of the acidizing process and PVBT extraction methodology including porosity/permeability and mineralogy heterogeneity. In: SPE International Symposium and Exhibition on Formation Damage Control. Lafayette, Louisiana: SPE. doi:10.2118/151823-MS.

Economides, M.J. & Nolte, K.G., 1989, Well analysis before and after fracture stimulation. In: The Centennial Symposium Petroleum Technology into the Second Century. Socorro, New Mexico: SPE. doi:10.2118/20153-MS.

Fedorov, K.M., Smirnov, A.S. & Kremieva, T.A., 2010, Carbonate acidizing: Conjunction of macro and micro scale investigations. In: Russian Oil & Gas Technical Conference and Exhibition. Moscow, Russia: SPE. doi:10.2118/136409-MS.

Fredd, C.N. & Fogler, H.S., 1996, The existence of an optimum Damkohler number for matrix stimulation of carbonate formations. In: SPE European Formation Damage Conference. The Hague, Netherlands: SPE. doi:10.2118/38167-MS.

Fredd, C.N., & Fogler, H.S., 2000a, Validation of carbonate matrix stimulation models. In: SPE International Symposium on Formation Damage Control. Lafayette, Louisiana: SPE. doi:10.2118/58713-MS.

Fredd, C.N., & Fogler, H.S., 2000b, Dynamic model of wormhole formation for effective skin reduction

during carbonate matrix acidizing. In: SPE Permian Basin Oil and Gas Recovery Conference. Midland, Texas: SPE. doi:10.2118/59537-MS.

Gdanski, R., 2018, Formation mineralogy impacts scale inhibitor squeeze designs. In: SPE European/ EAGE Annual Conference and Exhibition. Rome, Italy: SPE. doi:10.2118/113261-MS.

Ghalambor, A., & Economides, M.J., 2000, Formation damage abatement: A quarter century perspective. In: International Symposium on Formation Damage Control. Lafayette, Louisiana: SPE. doi:10.2118/58744-MS.

Glasbergen, G., & van den Akker, L., 2005, Field validation of acidizing wormhole models. In: SPE European Formation Damage Conference. Scheveningen, Netherlands: SPE. doi:10.2118/94695-MS.

Gong, M., & Yang, B., 1999, A quantitative model of wormholing process in carbonate acidizing. In: SPE Mid-Continent Operations Symposium. Oklahoma City, Oklahoma: SPE. doi:10.2118/52165-MS.

Kalfayan, L., 2008. Production enhancement with acid stimulation. Tulsa: PennWell.

Kalia, N., & Sarma, H.K., 2009, Wormhole formation in carbonates under varying temperature conditions. In: SPE European Formation Damage Conference. Scheveningen, Netherlands: SPE. doi:10.2118/121803-MS.

Klemin, D., Panga, M.K.R., & Valdes, J.R., 2015, Digital rock technology for quantitative prediction of acid stimulation efficiency in carbonates. In: SPE Annual Technical Conference and Exhibition. Houston, Texas: SPE. doi:10.2118/174807-MS.

Li, X., 2004, Rock texture and diagenetic evolution. Journal of Petroleum Science and Engineering, 42(1–2), pp.17–28.

Li, X. & Cheng, Y., 2004, Influence of rock texture on acidizing performance in carbonates. Journal of Petroleum Science and Engineering, 42(1–2), pp.29–40.

Lo, K.K., & Dean, R.H., 1989, Modelling of acid fracturing. SPE Journal, SPE-17110-PA.

Maheshwari, N., Maheshwari, A., & Sharma, M.M., 2013. 3-D simulation of carbonate acidization with HCl: Comparison with experiments. In: SPE Production and Operation Symposium. Oklahoma City, Oklahoma: SPE. doi:10.2118/164517-MS.

McDuff, D.R., Thompson, K.E., & Fogler, H.S., 2010, Understanding wormholes in carbonates: Unprecedented experimental scale and 3-D visualization. In: SPE Annual Technical Conference and Exhibition. Florence, Italy: SPE. doi:10.2118/134379-MS.

Morgenthaler, L.N., Zhu, D., Mou, J., & Hill, A.D., 2008, Effect of reservoir mineralogy and texture on acid response in heterogeneous sandstone. SPE Journal, SPE-102672-PA.

Muecke, T.W., 1982, Principles of acid stimulation. In: International Petroleum Exhibition and Technical Symposium of the Society of Petroleum Engineers. Beijing, China: SPE. doi:10.2118/10038-MS.

Navarette, R.C. & Lee, W.S., 1998, Laboratory and theoretical studies for acid fracture stimulation optimization. In: SPE Permian Basin Oil and Gas Recovery Conference. Midland, Texas: SPE. doi:10.2118/39776-MS.

Panga, M.K.R., Worley, J.B., & Fredd, C.N., 2004, A new model for predicting wormhole structure and formation in acid stimulation of carbonates. In: SPE International Symposium and Exhibition on Formation Damage Control. Lafayette, Louisiana: SPE. doi:10.2118/86517-MS.

Santosa, H., & Putra, R., 2018, Carbonate acidizing in Indonesian reservoirs. LEMIGAS Petroleum & Gas Bulletin, 52(2), pp.45–57.

Siregar, B., & Wibowo, S., 2019, Laboratory evaluation of acidizing fluid for Indonesian carbonate formations. LEMIGAS Petroleum & Gas Bulletin, 53(1), pp.12–25.

Settari, A., 1993, Modelling of acid-fracturing treatments. SPE Journal, SPE-21870-PA.

Shafiq, M.U., Ben Mahmud, H.K., & Arif, M., 2018, Mineralogy and pore topology analysis during matrix acidizing of tight sandstone and dolomite formations using chelating agents. Journal of Petroleum Science and Engineering, 171, pp.1126–1138. doi:10.1016/j.petrol.2018.09.027.

Turnip, J.F., Yasutra, A., Maulana, F., & Mustaqim, S.D., 2024, Mature Field and Well Revitalization:

Selection of Matrix Acidzing Candidates. Scientific Contributions Oil and Gas, 47 (1). https://doi.org/10.29017/SCOG.47.1.1613

Wei, W., Varavei, A., Sanaei, A., & Sepehrnoori, K., 2019. Geochemical modeling of wormhole propagation in carbonate acidizing considering mineralogy heterogeneity. Scientific Contributions Oil & Gas, 47(3), pp.101–110. doi:10.1007/s13399-019-00569-8.

Wibowo, A.S., (2013), Integration of Geology and Petroleum Engineering Aspects for Carbonates Rock Typing, Scientific Contributions Oil and Gas, 36 (1). https://doi.org/10.29017/SCOG.36.1.650

Xiao, J., Zhu, D., & Hill, A.D., 2019,Effect of heterogeneity in mineralogy distribution on acid fracturing efficiency. Scientific Contributions Oil & Gas, 47(3), 111–123. https://doi.org/10.1007/s13399-019-00570-5. , equalize columns on the last page.